Tracking the light-driven layer stacking of graphene oxide

Supplementary materials

Masaki Hada[1,2*†], Satoshi Ohmura[3†], Yuki Yamamoto[1†], Yoshiya Kishibe[1], Wataru Yajima[1], Ryo Shikata[1], Tomohiro Iguchi[4], Keishi Akada[1], Shoji Yoshida[1], Jun-ichi Fujita[1], Shin-ya Koshihara[5], Yuta Nishina[4,6*]

[1]Faculty of Pure and Applied Sciences, University of Tsukuba, Tsukuba 305-8573, Japan.
[2]Tsukuba Research Center for Energy Materials Science (TREMS), University of Tsukuba, Tsukuba 305-8573, Japan.
[3]Faculty of Engineering, Hiroshima Institute of Technology, Hiroshima 731-5193, Japan.
[4]Graduate School of Natural Science and Technology, Okayama University, Okayama 700-8530, Japan.
[5]School of Science, Tokyo Institute of Technology, Tokyo 152-8551, Japan.
[6]Research Core for Interdisciplinary Sciences, Okayama University, Okayama 700-8530, Japan.

[*]Emails:
hada.masaki.fm@u.tsukuba.ac.jp (Masaki Hada),
nisina-y@cc.okayama-u.ac.jp (Yuta Nishina)

[†]These authors equally contributed.

Supplementary Note 1 (Note S1)

We performed population analysis by expanding the electronic wave functions in the atomic-orbital basis sets[S1,S2]. Here, we describe a formulation of the population analysis based on a plane-wave basis set with ultrasoft pseudopotentials. Note that a generalization of the formulation to the projector-augmented-wave method is straightforward.

To project the self-consistent wave functions $\psi_n(\boldsymbol{r})$ of the *n*th electronic state obtained with the plane-wave basis into the subspace generated by the atomic basis $\{\phi_\mu\}$, the projection operator $\hat{P}$ is defined as[S3–S5],

$$\hat{P} = \sum_{\mu,\nu} |\phi_\mu\rangle\, S^{-1}_{\mu\nu} \langle\phi_\nu|\hat{s}, \tag{S1}$$

where

$$S_{\mu\nu} = \langle\phi_\mu|\hat{s}|\phi_\nu\rangle \tag{S2}$$

and

$$\hat{s} = 1 + \sum_{\mu,\nu} q_{\mu\nu} |\beta_\mu\rangle\langle\beta_\nu| \tag{S3}$$

with β_μ and $q_{\mu\nu}$ being the localized functions and the augmentation charges, respectively, in the ultrasoft pseudopotential.[S6]

By operating $\hat{P}$ on $\psi_n(\boldsymbol{r})$, the projected wave functions $\chi_n(\boldsymbol{r})$ are obtained as

$$|\chi_n\rangle = \hat{P}|\psi_n\rangle = \sum_\mu |\phi_\mu\rangle C_{\mu n}\,. \tag{S4}$$

where

$$C_{\mu n} = \sum_\nu S^{-1}_{\mu\nu}\, \langle\phi_\nu|\hat{s}|\psi_n\rangle. \tag{S5}$$

Generally, $\chi_n(\boldsymbol{r})$ are not orthogonalized; $R_{nm} = \langle\chi_n|\hat{s}|\chi_m\rangle \neq \delta_{nm}$,

To ensure charge conservation, the dual of $\chi_n(\boldsymbol{r})$ is introduced as,

$$|\chi^n\rangle = \sum_m |\chi_m\rangle R^{-1}_{mn} = \sum_\mu |\phi_\mu\rangle C^{\mu n} \tag{S6}$$

where

$$C^{\mu n} = \sum_m C_{\mu m}\, R^{-1}_{mn} \tag{S7}$$

so that

$$\langle\chi^n|\hat{s}|\chi_m\rangle = \delta_{nm}. \tag{S8}$$

For the *n*th electronic state, the partial gross atomic population $N^{(n)}_\mu$ associated with the μth atomic basis function and the partial bond-overlap population $O^{(n)}_{\mu\nu}$ associated with the μth and νth atomic basis functions are defined as

$$N_{\mu}^{(n)} = \sum_{\nu} C^{\nu n} S_{\nu\mu} C_{\mu n} \tag{S9}$$

and

$$O_{\mu\nu}^{(n)} = \frac{1}{2}\left(C^{\mu n} S_{\mu\nu} C_{\nu n} + C^{\nu n} S_{\nu\mu} C_{\mu n}\right), \tag{S10}$$

respectively.

By summing $N_{\mu}^{(n)}$, the gross atomic population N_i for the ith atom is obtained as follows:

$$N_i = \sum_{n} \sum_{\mu \in i} f_n N_{\mu}^{(n)}, \tag{S11}$$

where f_n is the electronic occupation number of the nth electronic state.

The gross charge of the ith atom Q_i is given by

$$Q_i = Z_i - N_i, \tag{S12}$$

where Z_i is the total number of valence electrons of a free neutral atom.

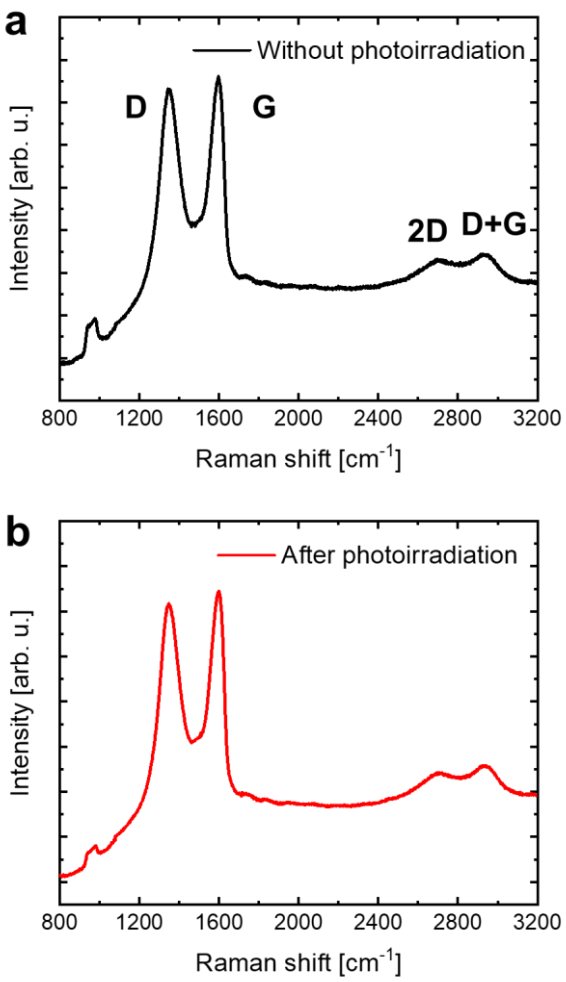

Supplementary Figure 1 (Figure S1). Raman spectra of graphene oxide without (a) and after (b) UV photoirradiation at an incident fluence of 4 mJ/cm^2. In both spectra, D, G, 2D, and D+G peaks are observed as indicated in the figure; however, the difference between these spectra is hardly observable due to the incomplete recovery of the graphene framework. The peak at a Raman shift of ~1000 cm^{-1} is derived from the Si substrate.

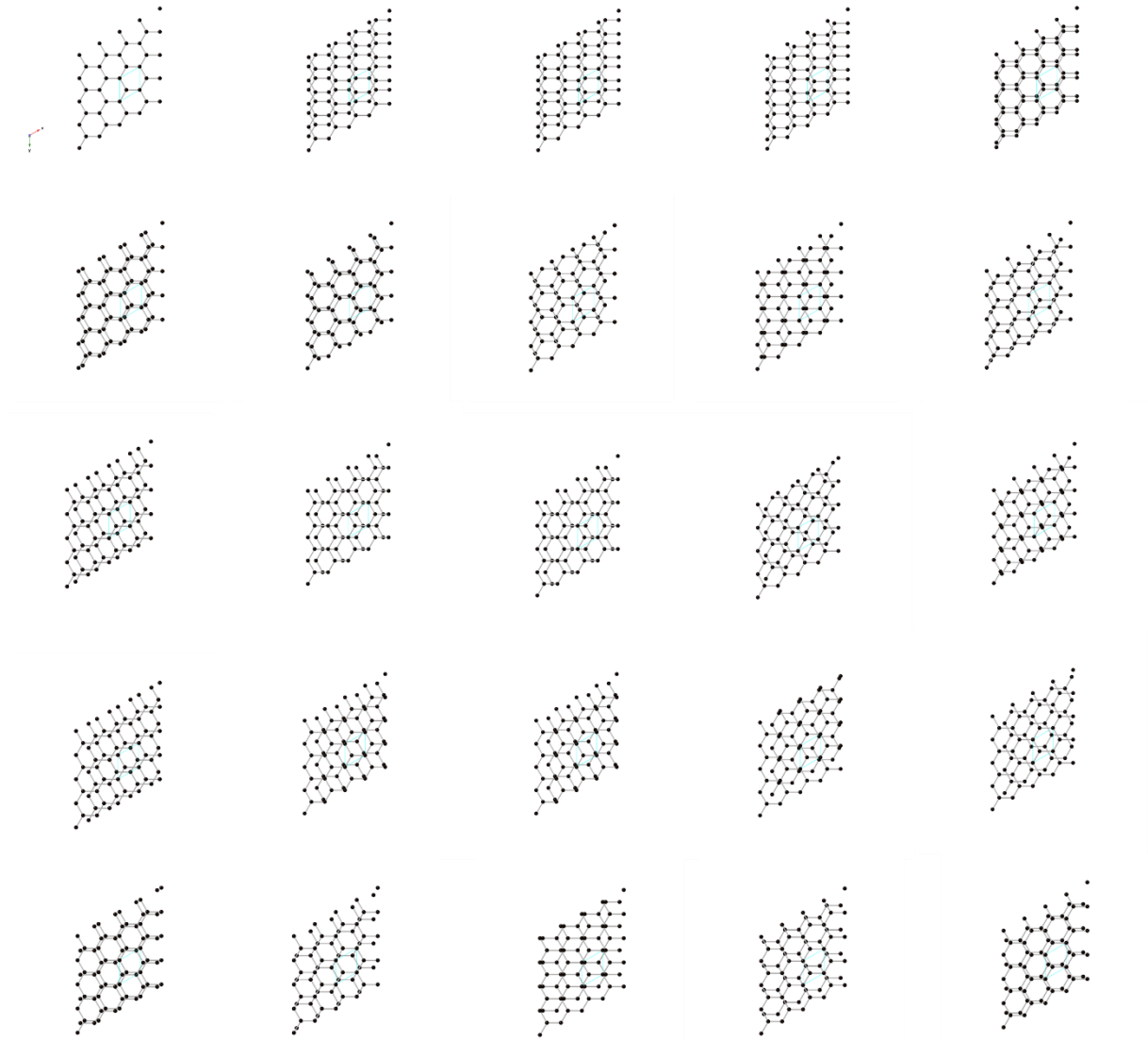

Supplementary Figure 2 (Figure S2). Randomly oriented 25-graphene model structures for the calculation of the electron diffraction patterns.

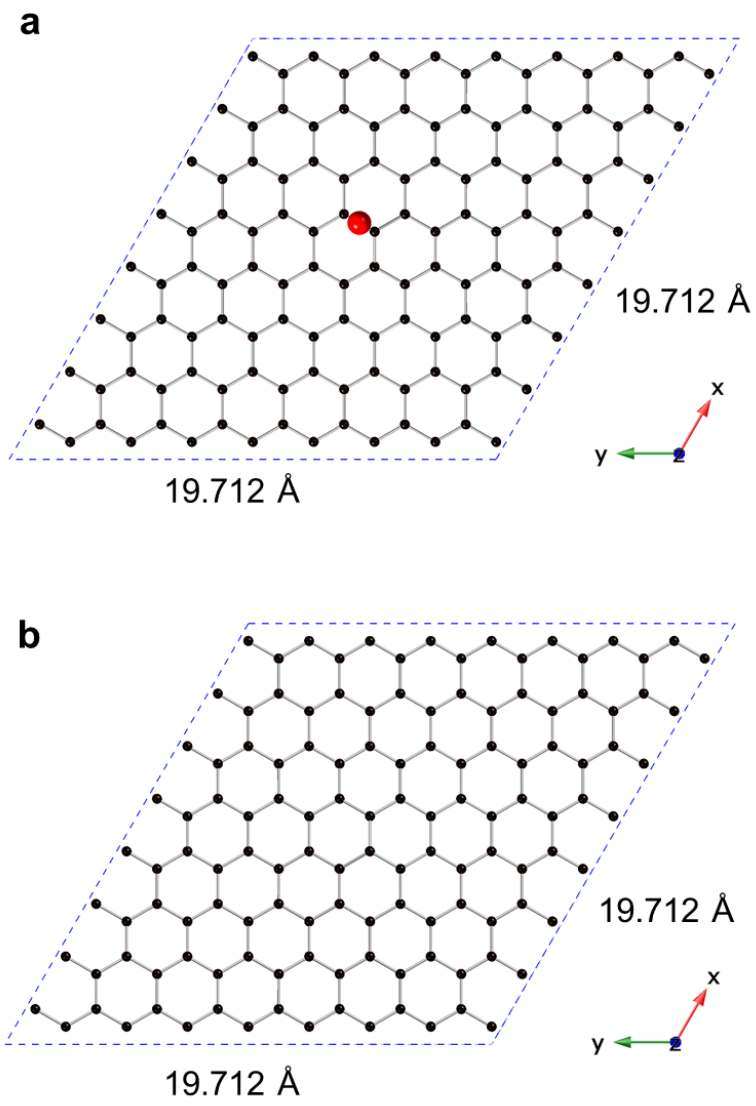

Supplementary Figure 3 (Figure S3). (a) The model GO layer based on an 8 × 8 graphene supercell (128 carbon atoms) with epoxy-functional group oxygen. (b) The model graphene layer based on an 8 × 8 graphene supercell. The upper and lower layers of the model GO bilayer are (a) and (b). One side length of the supercell is 19.712 Å.

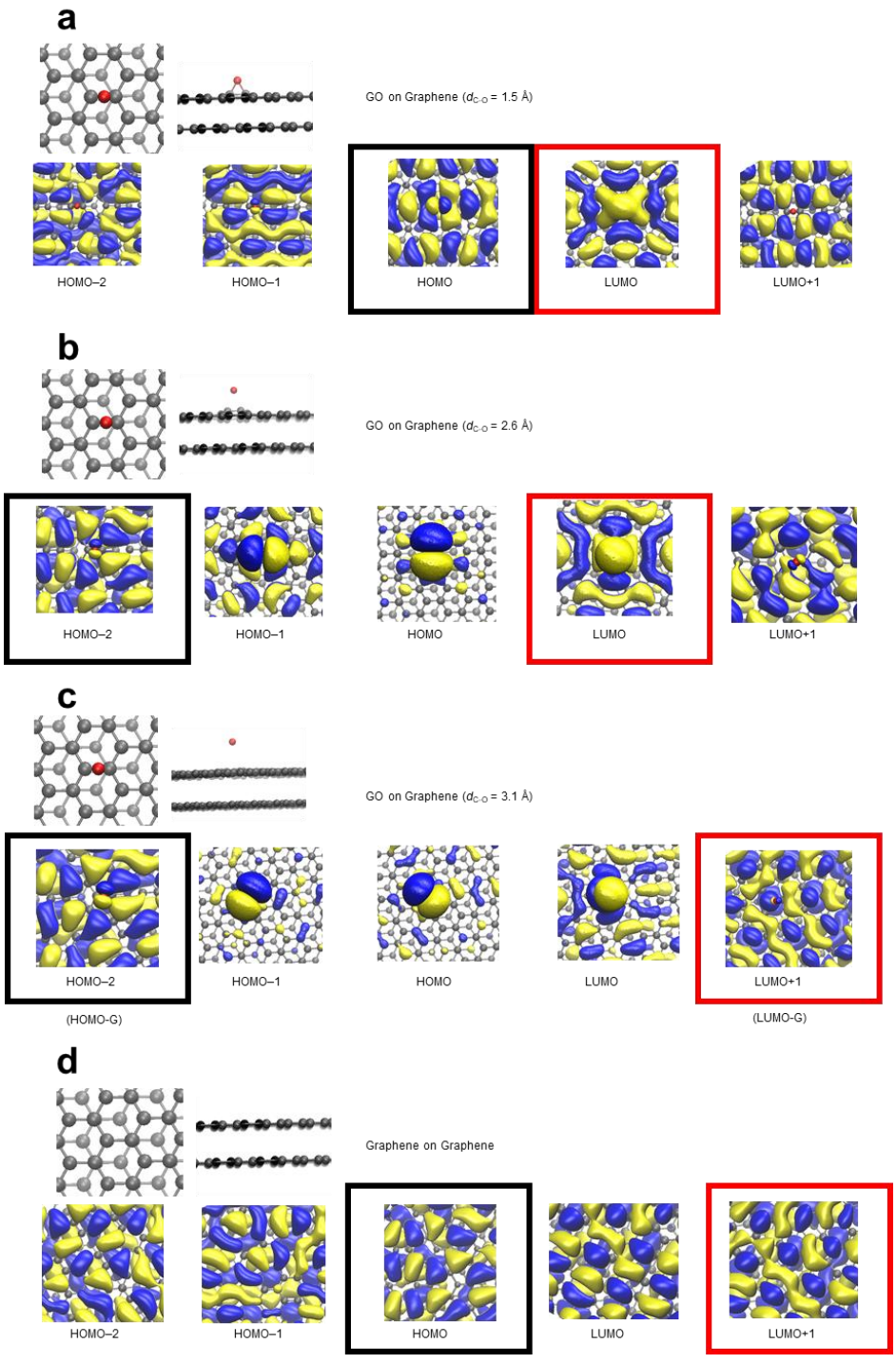

Supplementary Figure 4 (Figure S4). (a–d) Highest occupied molecular orbitals (HOMOs) and lowest unoccupied molecular orbitals (LUMOs) of the bilayer graphene models in detail. The HOMOs and LUMOs surrounded by black and red circles are the corresponding orbitals of the graphene model shown in the main text.

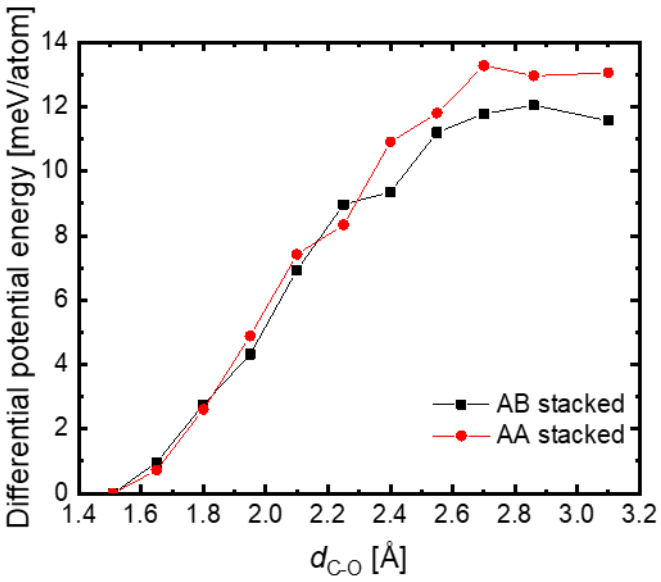

Supplementary Figure 5 (Figure S5). Potential energy as a function of $d_{C\text{-}O}$ for AB stacking and AA stacking. Structural optimization is not performed in each $d_{C\text{-}O}$. The origin of the axis representing energy is taken to be the energy at distance = 1.5 Å of each system. Since a large $d_{C\text{-}O}$ is unstable, energy increased with increasing $d_{C\text{-}O}$ for all the stacking patterns. However, the increasing ratio of AB stacking is smaller when $d_{C\text{-}O}$ exceeds 2.4 Å. This result originates from the conflict between the destabilization of GO and stacking stabilization, which indicates that the removal of epoxy-oxygen enhances AB stacking.

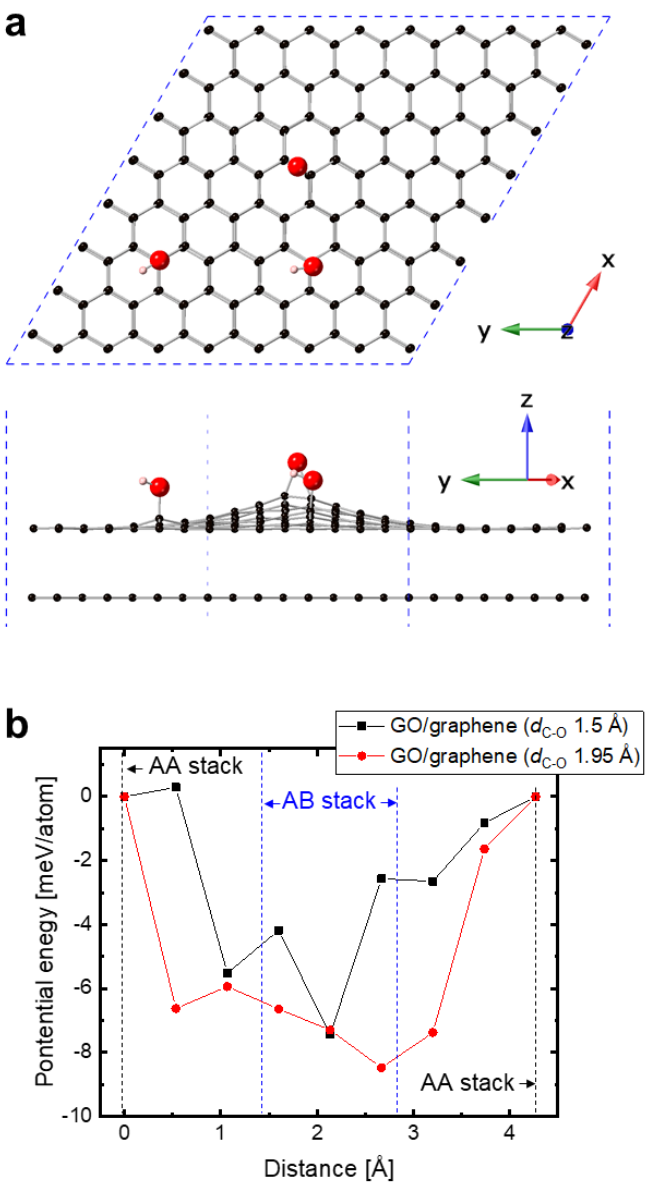

Supplementary Figure 6 (Figure S6). The effects of hydroxyl-functional groups around the epoxy-functional group on the basal plane of GO. (a) One of the potential structures of the model GO bilayer with an epoxy-functional group with the presence of two hydroxyl-functional groups. (b) The potential energy with sliding the upper layer of the model GO bilayer. The potential energy removing the epoxy-oxygen shows a steep local minimum around the position of the AB stacking.

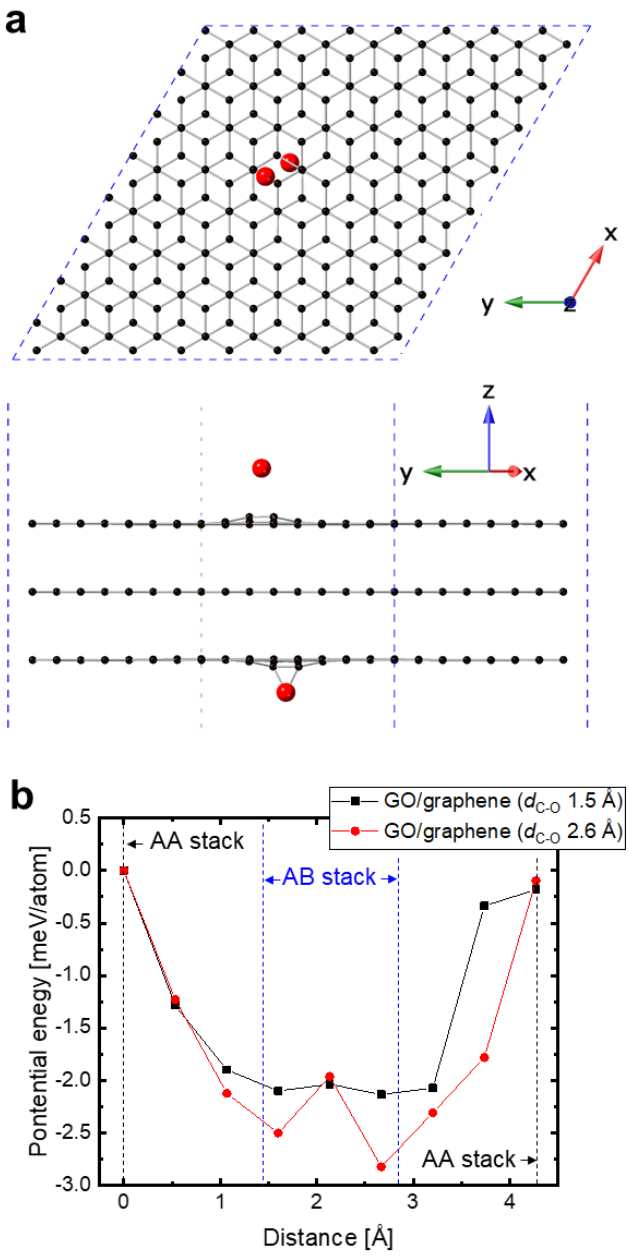

Supplementary Figure 7 (Figure S7). (a) One of the potential structures of the model GO trilayer with an epoxy-functional group. (b) The potential energy with sliding the uppermost layer of the model GO trilayer. The potential energy removing the epoxy-oxygen shows a steep local minimum around the position of the AB stacking.

Supplementary references

S1. R. S. Mulliken, Electronic population analysis on LCAO-MO molecular wave functions. II. Overlap populations, bond orders, and covalent bond energies. *J. Chem. Phys.* **23**, 1841–1846 (1955).

S2. F. Shimojo, A. Nakano, R. K. Kalia, P. Vashishta, Electronic processes in fast thermite chemical reactions: A first-principles molecular dynamics study. *Phys. Rev. E* **77**, 066103 (2008).

S3. D. Sánchez-Portal, E. Artacho, J.M. Soler, Analysis of atomic orbital basis sets from the projection of plane-wave results. *J. Phys. Condensed. Matter* **8**, 3859–3880 (1996).

S4. M.D. Segall, R. Shah, C.J. Pickard, M.C. Payne, Population analysis of plane-wave electronic structure calculations of bulk materials. *Phys. Rev. B* **54**, 16317–16320 (1996).

S5. F. Shimojo, K. Hoshino, Y. Zempo, Ab initio molecular-dynamics simulations of anomalous structural change in liquid tellurium under pressure. *J. Phys. Soc. Jpn.* **72**, 2822–2828 (2003).

S6. D. Vanderbilt, Soft self-consistent pseudopotentials in a generalized eigenvalue formalism. *Phys. Rev. B* **41**, 7892–7895 (1990).